ACI STRUCTURAL JOURNAL TECHNICAL PAPER

Title no. 99-S9

Behavior of Three-Dimensional Reinforced Concrete Shear Walls

by Daniel Palermo and Frank J. Vecchio

Results from two large-scale flanged shear walls tested under static cyclic displacements are presented. The objectives of the tests were to provide insight into the behavior of shear walls under cyclic displacements, and more importantly, to provide data to help corroborate constitutive models for concrete exposed to arbitrary loading conditions. The results indicated that the presence of an axial load, although relatively small, and the stiffness of flange walls have a significant effect on the strength, ductility, and failure mechanisms of the shear walls. Finite element analyses using provisional constitutive models are also provided to show that the procedures employed are stable, compliant, and provide reasonably accurate simulations of behavior. The analyses presented also indicated that two-dimensional analyses capture main features of behavior, but three-dimensional analyses are required to capture some important second-order mechanisms.

Keywords: load; reinforced concrete; shearwall.

INTRODUCTION

To assess the seismic safety factor of nuclear reactor buildings, the Nuclear Power Engineering Corporation of Japan (NUPEC) recently conducted an extensive experimental investigation. Two large-scale flanged shear walls were subjected to dynamic loading using a high-performance shaking table. The results of the tests were made available to participants of the Seismic Shear Wall International Standard Problem (SSWISP) Workshop.[1]

It became evident from the competition results that the ability to predict the peak strength of shear walls under seismic excitations was not well established. More importantly, however, was the apparent inability of leading researchers to accurately predict structural ductility. The predictions were based on finite element method (FEM) static monotonic and static cyclic analyses, FEM dynamic analyses, simplified static and dynamic analyses, and lumped-mass dynamic analyses. Figure 1(a) and (b) show the analytical results of the predicted maximum load and the predicted displacement at maximum load for the FEM static analyses, respectively.

The results indicated that the methods and models used were able to predict the maximum load more accurately than the displacement at maximum load. The maximum load reported by NUPEC was 1636 kN, and the corresponding displacement was 10.96 mm. The analytical maximum load results varied between 65 to 115% of the experimental value, with the majority of the participants underestimating the peak strength. The variation was, however, smaller than that of the displacement at the maximum load. The range in predicted displacements was from 35 to 180% of the actual amongst those participants who submitted results. Again, the majority of predictions underestimated the ductility of the shear walls.

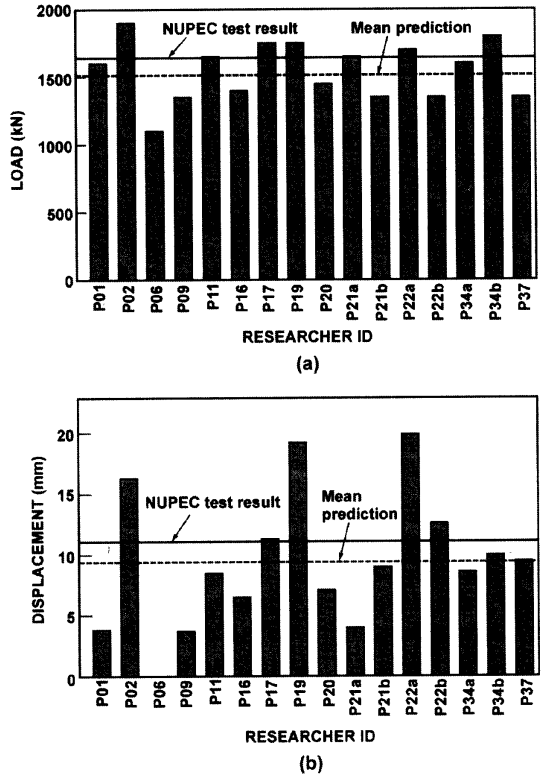

Fig. 1—NUPEC results: (a) maximum predicted load; and (b) predicted displacement at maximum load.

These apparent difficulties with accurately modeling ductility led to large-scale testing of flanged shear walls at the University of Toronto. The purpose of this experimental program was to investigate the behavior of shear walls under cyclic loading, to provide test data to formulate improved cyclic models, and to assess current capabilities in predicting structure ductility using in-house FEM programs.

The main objective of this paper is to present and discuss the results of the experimental program conducted at the University of Toronto. Analyses using provisional constitutive models are presented to show that computational procedures can be stable and compliant, and can provide reasonably accurate simulations of behavior. A companion paper will discuss the theoretical models and finite element studies.

ACI Structural Journal, V. 99, No. 1, January-February 2002.
MS No. 01-031 received February 2, 2001, and reviewed under Institute publication policies. Pertinent discussion will be published in the November-December 2002 *ACI Structural Journal* if received by July 1, 2002.

Daniel Palermo, *PEng, is a doctoral candidate in the Department of Civil Engineering, University of Toronto, Toronto, Ontario, Canada. He received his MASc and BASc from the University of Toronto in 1998 and 1995, respectively. His research interests include constitutive modeling of concrete subjected to cyclic loading and experimental testing of shear walls.*

ACI member **Frank J. Vecchio** *is Professor and Associate Chair in the Department of Civil Engineering at the University of Toronto. He is a member of Joint ACI-ASCE Committee 447, Finite Element Analysis of Reinforced Concrete Structures. His research interests include nonlinear analysis and design of concrete structures, constitutive modeling, assessment, and repair and rehabilitation of structures.*

Table 1—Concrete material properties

	f_c', MPa		ε_c', MPa ($\times 10^{-3}$)	
Zone	DP1	DP2	DP1	DP2
Web wall	21.7	18.8	2.04	2.12
Flange wall	21.7	18.8	2.04	2.12
Top slab	43.9	38.0	1.93	1.96
Bottom slab	34.7	34.7	1.66	1.66

Table 2—Reinforcement material properties

Zone	Type	Diameter, mm	ε_{sy}, ($\times 10^{-3}$)	f_{sy}, MPa	f_{su}, MPa
Web wall	D6	7	3.18	605	652
Flange wall	D6	7	3.18	605	652
Top slab	No. 30	29.9	2.51	550	696
Bottom slab	No. 30	29.9	2.51	550	696

RESEARCH SIGNIFICANCE

The inability of leading researchers to accurately estimate load-displacement responses of the NUPEC shear walls indicated that significant work and attention should be focused towards formulating improved hysteretic response and ductility models. Ensuring that current and future analytical models provide reasonably accurate simulations of behavior requires experimental data for corroboration. Experimental data can also provide useful information for better understanding the behavior of shear walls under cyclic loading conditions. The experimental results presented herein will augment the literature with tests in which the response was dominated by shear related mechanisms and tests involving more complex wall configurations.

EXPERIMENTAL PROGRAM

An experimental program was recently conducted on two large-scale flanged reinforced concrete shear walls. Two specimens, DP1 and DP2, were tested. The original test specimens were also repaired and tested to failure: DP1R and OH respectively. Testing of Specimens DP1[2] and DP1R[3] consisted of imposed lateral cyclic displacements under a constant applied axial load. The second series of tests differed in terms of loading. DP2[4] was subjected to lateral cyclic displacements without axial load, and OH[5] consisted of lateral monotonic displacements under an applied axial load.

The specimens were constructed with stiff top and bottom slabs. The top slab (4415 x 4000 x 640 mm) served to distribute the horizontal and axial loads to the walls of the structure. The bottom slab (4415 x 4000 x 620 mm), clamped to the laboratory strong floor, simulated a rigid foundation. The slabs were reinforced with No. 30 deformed reinforcing bars at a spacing of 350 mm in each direction, with a top and bottom layer. The web wall, 2885 mm in length, 2020 mm in height,

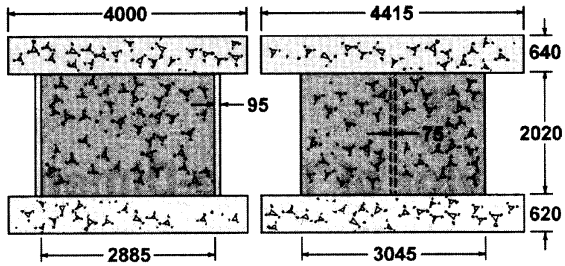

Fig. 2—Test specimen details.

and 75 mm in thickness, was reinforced with D6 reinforcing bars. The bars were spaced 140 mm horizontally and 130 mm vertically in two parallel layers. The two flange walls were approximately 3045 mm long, 2020 mm high, and 95 mm thick for DP1 and 100 mm thick for DP2. The flanges were also reinforced with D6 reinforcing bars, spaced 140 mm horizontally and 130 mm vertically near the web wall and 355 mm near the tips of the flanges. The concrete clear covers in the walls and slabs were 15 and 50 mm, respectively. Dimensional details of the walls are shown in Fig. 2, and the reinforcement layout for the web and flange walls are given in Fig. 3.

The two shear walls had identical dimensions and reinforcement, and were similar to the NUPEC specimen. The concretes used in DP1 and DP2 were supplied by a local ready-mix plant and were of comparable strength. Details of the concrete and reinforcement properties are given in Table 1 and 2, respectively. Material properties for DP1R and OH are reported elsewhere.[6]

Each wall was subjected to a combination of lateral and axial loading using the testing apparatus shown in Fig. 4, except DP2, for which the axial load was removed. The constant applied axial load of 940 kN, chosen to be consistent with the loading of the NUPEC tests, was first applied through two spreader beams clamped over the flanges by four 600-kN actuators. The self-weight of the top slab provided an additional 260 kN. After the total axial force was applied, the specimens were displaced laterally by 1-mm increments. For the cyclic tests, two repetitions at each displacement level were imposed. The lateral loading criteria were representative of a severe cyclic loading regime, and allowed necessary hysteresis data to be obtained for corroborating cyclic loading models. The lateral displacements were imposed by two 1000-kN actuators that were mounted to the laboratory strong wall and connected to the top slab of the specimens. (The strong wall, shown in Fig. 4, was located on the north side of the test specimens.) A single linear variable displacement transducer (LVDT), located at the midheight of the top slab, was used to measure the absolute top slab movements. Two additional LVDTs were placed at the opposite end of the structure to monitor twisting of the top slab. Testing of the original specimens was halted prior to any catastrophic failure so that a simple and effective rehabilitation could be implemented.

The specimens were mounted with Zurich targets to measure concrete surface strains, linear variable displacement transducers (LVDTs) to measure displacements, and strain gages to measure strains in the reinforcement. Eighteen Zurich targets were mounted on the flange walls and an additional four targets were placed at each toe of the east face of the web wall. (The toe refers to the lower corners of the web wall

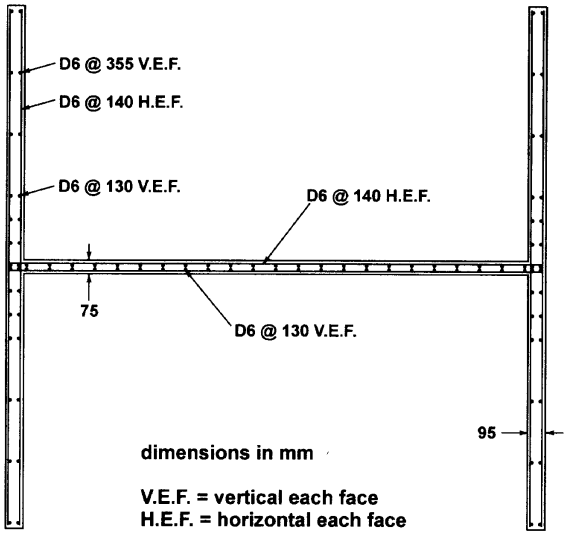

Fig. 3—Top view of wall reinforcement.

where the base slab and flange wall connect, where stresses are a maximum and crushing of the concrete or yielding of the reinforcement are likely to initiate.) A total of 21 LVDTs were mounted to the specimen to measure the horizontal displacement of the top slab, the relative displacement of the top to bottom slab, the horizontal displacement at the midheight of the flange walls, the bond slip of the walls with the base slab, and the slippage of the base slab relative to the strong floor. Additional LVDTs were installed at each toe of the west face of the web wall. The reinforcement strains were monitored with the use of 40 strain gages. In the web wall, gages were mounted on the reinforcement along the base of the web wall and near the midheight of the web. For the flange walls, strain gages were used to measure the strains near the base of the walls, and near the midheight of the flanges. For the horizontal reinforcement, strain gages were placed on the reinforcing bars located at the midheight of the flange and web walls. Load cells were also connected to the six actuators to monitor the load. Each displacement level was held for 5 min to measure crack size, mark cracks, take photographs of the cracking patterns, and record Zurich readings. The strain gages and LVDTs provided continuous readings.

TEST RESULTS

The primary focus herein is on the original test specimens, DP1 and DP2. The test results include cracking characteristics, load-deformation responses, and reinforcement strains. Comprehensive test results are provided elsewhere.[2,4]

Cracking characteristics

The two specimens exhibited similar cracking patterns throughout the course of testing. Diagonal cracking initiated at a lateral load of –408 kN and a corresponding displacement of –0.63 mm for DP1, and –256 kN at a displacement of –0.47 mm for DP2. These cracks surfaced during the first excursion to –1 mm. (The negative quantities refer to pulling of the specimen toward the laboratory strong wall.) Similar loads and displacements were recorded at the onset of diagonal cracking in the positive direction. Diagonal cracks continued to appear with increasing displacement. The diagonal cracks generally extended the full height of the web wall, from the top right corner to the bottom left corner in the negative direction, generally inclined at 45 degrees. In the positive direction,

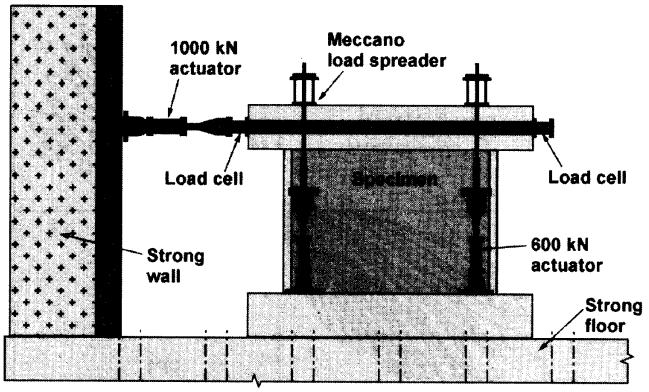

Fig. 4—Testing apparatus.

these cracks traveled orthogonal to the negative diagonal cracks. New cracks typically appeared during the first excursion of each displacement level. During the second excursion, smaller secondary cracks formed between the major diagonal cracks. By the end of Cycle 4 (4 mm of displacement), the web wall was essentially fully cracked. During Cycle 5, there was visual evidence of slipping along the crack surfaces. During the unloading phase, the crack surfaces were not capable of realigning, which caused a grinding of the two surfaces. The result was localized crushing along the crack surfaces throughout the web wall, and this continued to the end of testing. The maximum diagonal crack widths recorded were 1.0 mm for DP1 and 0.6 mm for DP2, observed during cycles 13 and 9, respectively. With the two specimens, cracks that formed during later stages generally remained parallel to the first diagonal crack, and thus there was no visible evidence of cracks rotating.

Similar flexural cracking patterns were observed on the flange walls of DP1 and DP2. For DP1, the first crack in the flange walls appeared during the first excursion to 3 mm, on the outside surface of the flange farthest from the strong wall near the flange-web wall intersection. The crack formed a U-shaped pattern, and it surfaced approximately 1/3 of the wall height from the top slab. The approximate load and displacement at the onset of cracking were –819 kN and –2.9 mm, respectively. The maximum flexural crack width of 1.1 mm was recorded during the first excursion to 12 mm of displacement. For DP2, the first flexural crack surfaced on the far flange wall during the first excursion to 2 mm. The crack surfaced 1/4 of the height of the wall from the base slab, extended the full width of the flange, and propagated through the thickness of the flange. The load and displacement recorded at cracking were –385 kN and –1.19 mm, respectively. A maximum flexural crack of 1 mm was measured during the first excursion to 9 mm in Specimen DP2. By the end of testing, 4 to 5 major flexural cracks evenly spaced along the height were evident on the flange walls of the two specimens, extending the full width and thickness of the wall. Further flexural cracking was concentrated near the flange-web wall intersection. Vertical cracks extending the full height of the flange walls were also visible at the flange-web wall connection. The location of the maximum flexural crack width differed for the two test specimens. For DP1, the maximum crack width was measured near the midheight of the flange, and for DP2, about 50 mm from the top slab. These crack locations played key roles in determining the mechanisms of failure for the two walls.

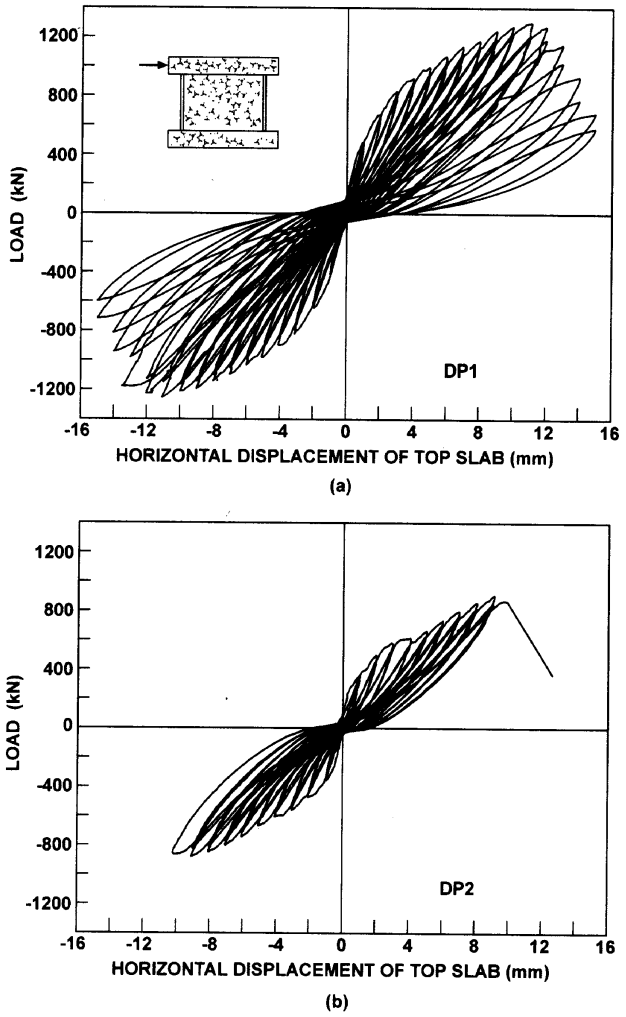

Fig. 5—Observed load-deformation response: (a) Specimen DP1; and (b) Specimen DP2.

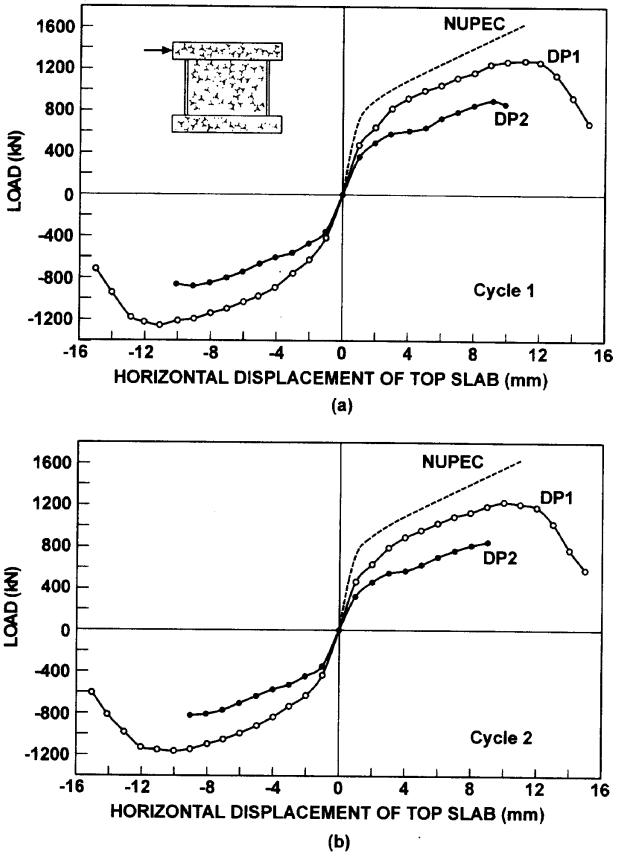

Fig. 6—Envelope response: (a) first excursion; and (b) second excursion.

Load-deformation response

Three LVDTs were mounted to the midheight of the top slab to monitor the displacement of the structure. Analysis of the readings indicated that the walls remained stable and an insignificant amount of twisting was recorded.

Testing was terminated after the completion of 15 mm of displacement for DP1. At this point, a significant portion of the descending branch of the load-deformation response had been attained. Maximum loads were recorded in the first excursion to 11 mm. The maximum load and corresponding displacement in the positive direction were 1298 kN and 11.14 mm, respectively, and –1255 kN and –11.09 mm for the negative direction loading. Specimen DP2, without axial load, was not capable of sustaining a ductile post-peak response. This shear wall failed during the first excursion to 10 mm. Maximum loads were recorded during the first excursion to 9 mm. In the positive direction, a load of 904 kN at a corresponding displacement of 9.15 mm was recorded, and a load of –879 kN at a displacement of –9.08 mm was attained in the negative direction. The full load-deformation responses of DP1 and DP2 are shown in Fig. 5. The maximum loads for each displacement level, forming an envelope response, are plotted in Fig. 6 with the NUPEC results for later discussion.

The elongations of the flange wall nearest the laboratory strong wall are plotted in Fig. 7(a) and (b) for DP1 and DP2, respectively. The elongation is a second-order phenomenon, but is useful in understanding behavior. It can be used to determine the extent of cracking and ratcheting in the flange walls. (Ratcheting is a term used to describe the vertical stretching of the flange wall due to the irrecoverable strains that accumulate in the post-yield cycles.) DP1 experienced 4.18 mm of extension under a horizontal load of 1270 kN, occurring during cycle 12, and DP2 had an extension of 4.11 mm at a load of 868 kN just prior to failure. In compression, however, DP1 demonstrated more contraction to its original height than did DP2. The relatively insignificant residual displacements at zero loads further indicated that yielding of the flexural reinforcement was not widespread and most likely was confined locally in the vicinity of cracks.

Bulging of the web wall is another interesting second-order mechanism. The bulging is a measure of the dilation of the web wall due to cracking and yielding of the reinforcement and indicates the extent of compression softening due to the existence of transverse tensile straining. High expansion results in an increased compression-softening effect in the web concrete and higher stresses in the web reinforcement and restraining flanges. LVDTs located at the midheight of the flange walls near the web recorded the bulging of the web wall. Figure 8 shows the bulging of DP2. A plot of the results for DP1 is unavailable. The maximum bulging of 6.52 mm for DP1 occurred during the first excursion to –13 mm of displacement, and the corresponding load was –1177 kN. The response was similar in the positive direction. For DP2, the bulging was also identical in the positive and negative directions. A maximum bulging of 4.62 mm at a load of –860 kN occurred during the first excursion to cycle 10. As can be noted, the hysteretic bulging was not significantly

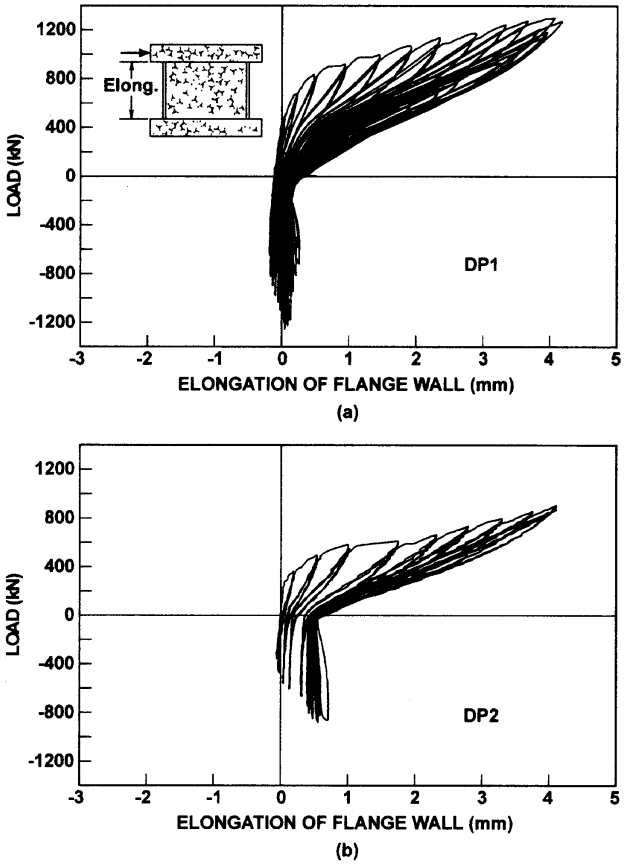

Fig. 7—Elongation of flange wall: (a) Specimen DP1; and (b) Specimen DP2.

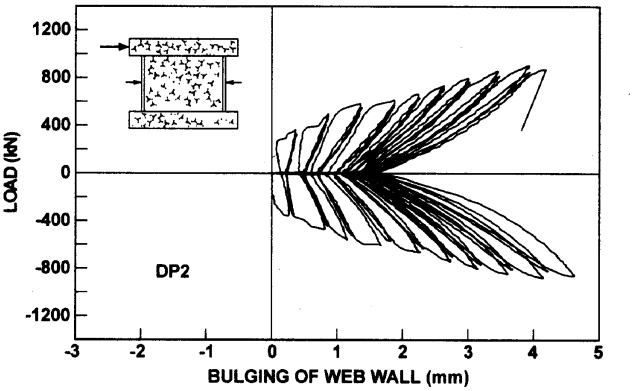

Fig. 8—Bulging of DP2 web wall.

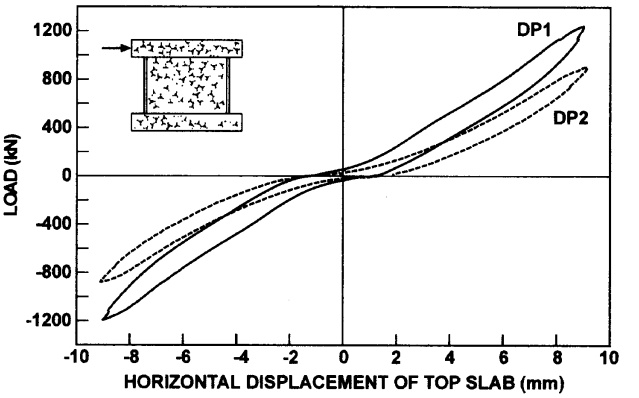

Fig. 9—Comparison of DP1 and DP2 responses at 9 mm of displacement.

pinched and retained large residual strains, suggesting that local strains in the web reinforcement were large and possibly in excess of yield.

Reinforcement strains

Of the 40 strain gages located in each of DP1 and DP2, only two strain gages in DP1 recorded strains in excess of yield, located on a horizontal reinforcing bar near the mid-height of the web wall. This does not necessarily indicate that reinforcing bars located elsewhere were not yielding. The Zurich targets for the two specimens recorded fairly large concrete surface strains in the flanges. These targets were located 250 mm from each of the slabs and at the mid-height of the wall, and were spread over the length of the flanges. Large strains were recorded throughout the flange walls by targets that surrounded cracks. Therefore, the flexural reinforcement likely was yielding locally at crack locations throughout the flange walls, but was not captured by any of the strain gages.

DISCUSSION OF RESULTS

The extensive data collected from DP1 and DP2 are extremely useful in understanding the behavior of shear walls, the effects of axial load, and the effects of flange walls.

Strength and deformation characteristics

The results indicated that the presence of a small amount of axial load had a significant effect on the behavior of the shear walls subjected to reversed cyclic displacements. The applied axial load of 940 kN on Specimen DP1 represented an axial stress of 1.18 MPa and was the equivalent of 5.4% of f_c'. DP2, without axial load, was only able to attain 70% of the maximum load resisted by DP1. DP2 did, however, have a cylinder compressive strength 13% lower than DP1. The maximum load resisted by DP2 occurred at a displacement of 80% of that experienced by DP1. The reduction in strength and ductility of DP2 cannot solely be attributed to the reduced compressive strength of the concrete. It is apparent that a small amount of axial load enhanced the performance of DP1. A comparison of the first excursion for Cycle 9 (peak load stage for DP2) for both specimens shown in Fig. 9 reveals some interesting trends. DP2 had a significantly lower loading and unloading stiffness. The residual strains were identical for both structures; and, as confirmed by other researchers,[7] this is a function of the maximum strain experienced. DP1 seemed to dissipate more energy than DP2, and the hysteresis loops of DP2 seemed to experience more pinching.

Failure mechanisms

The presence of axial load and the stiffness of the flange walls contributed to the sequence of failure of DP1 and DP2. The failure mechanisms of the two walls were unexpected and not consistent with failures of other shear walls in the literature.[8,9,10] The conventional thought on squat shear walls holds that failure can occur either by diagonal tension or diagonal compression.[11] Diagonal tension failure occurs when insufficient horizontal shear reinforcement is placed in the web section of the wall. Diagonal compression failure occurs when the shear stress on the web is large. In the latter case, the concrete in the toe region crushes, followed by a sliding shear plane extending along the base of the wall.

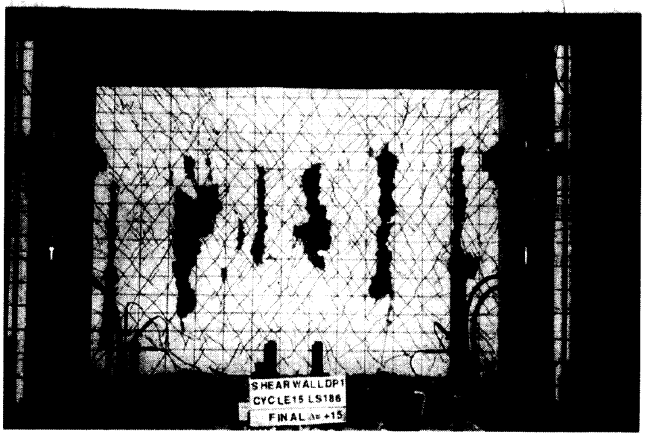

(a)

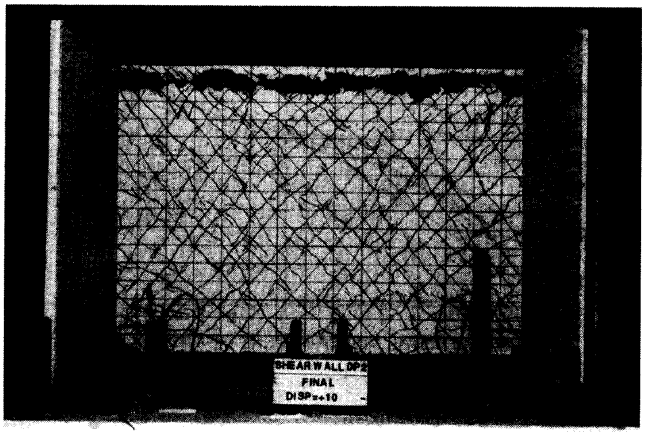

(b)

Fig. 10—Web wall at failure: (a) Specimen DP1; and (b) Specimen DP2.

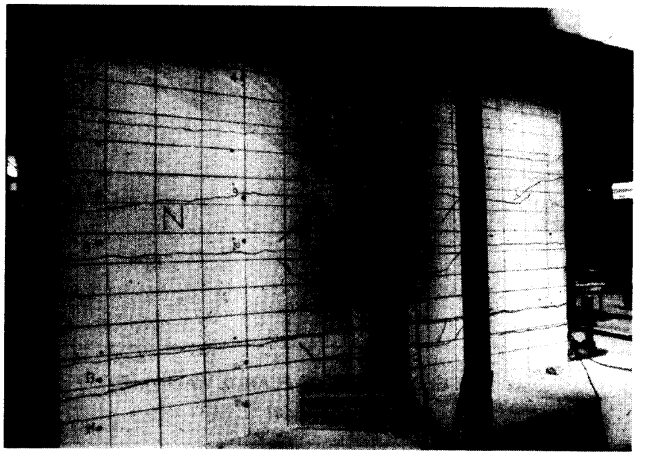

(a)

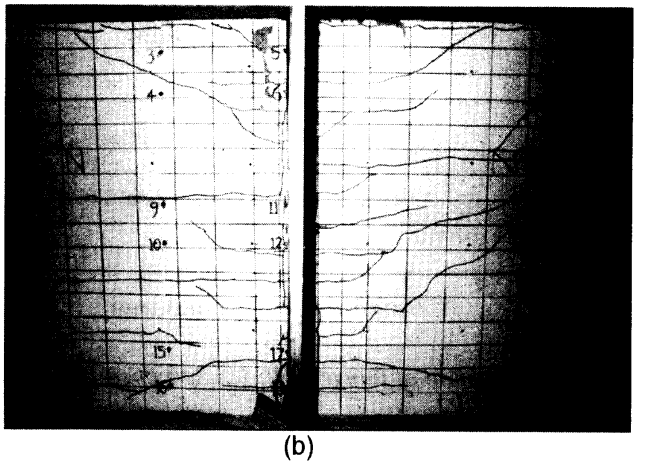

(b)

Fig. 11—Flange wall at failure: (a) Specimen DP1; and (b) Specimen DP2.

Testing of DP1 was terminated at 15 mm of displacement. The web wall's ability to resist the horizontal displacements was impaired beyond the peak load cycle (11 mm), and with each successive cycle, the integrity of the concrete continued to diminish. Six vertical planes of failure, equally spaced along the web wall, were evident (Fig. 10(a)). These planes began to form during 11 mm of displacement, near the toes of the web. The relatively undamaged and stiff flange walls provided restraint against the opening of diagonal cracks in the web wall, thus causing the formation of vertical slip planes. The crushing of the concrete along the slip planes was the result of grinding as adjacent surfaces slipped relative to each other. The flange walls experienced flexural cracking; otherwise, no other significant damage was visible. Failure ultimately involved severe crushing of the concrete over a widespread region of the web wall. Oesterle et al. reported a similar type of failure mechanism for a shear wall with stiff boundary elements.[12] Repair of Specimen DP1 involved a full depth replacement of the existing concrete in the web wall with new concrete.

Testing of DP2 was halted at 10 mm of displacement, at which point a sliding shear plane was evident in the web wall near the top slab. The mechanism leading to failure was initiated by yielding of the flexural reinforcement near the top slab. A maximum flexural crack width of 1 mm had been observed in this area. Prior to the formation of a sliding shear plane, crushing of the concrete at the top south corner of the web wall, followed by crushing at the top north corner was evident. On displacing the structure to +10 mm of displacement, a sudden sliding shear plane formed along the top of the web wall (Fig. 10 (b)). This failure plane extended the entire length of the web wall and caused a punching of the flange walls near the top slab. This appears to have been the result of the concrete being weaker near the top of the wall section, causing a zone of weakness. It can be noted that the concrete in the failure zone was of a brittle nature and reduced to a rubble-like material at failure, further suggesting a weaker concrete near the top slab. A post-peak response for DP2 was not realized due to the sudden failure after the peak load. Repair of DP2 consisted of a full depth replacement of the concrete in the web wall and a portion of the flange wall near the web-flange intersection. Figure 11 illustrates the damage experienced by the flange walls.

It is important to note that prior to failure of DP1 and DP2, concrete in the area of the toes near the base slab of the web walls was spalling, and there were also signs of crushing in these regions prior to the peak load cycle. The stiffness of the flange walls in DP1 restrained diagonal cracks from opening and from concentrating the crushing of the concrete in the toe area, and the apparently weaker concrete of DP2 near the top slab initiated failure away from the base of the web wall. Clearly, the stiffness of the flange walls played a key role in the failure mechanisms of the two specimens.

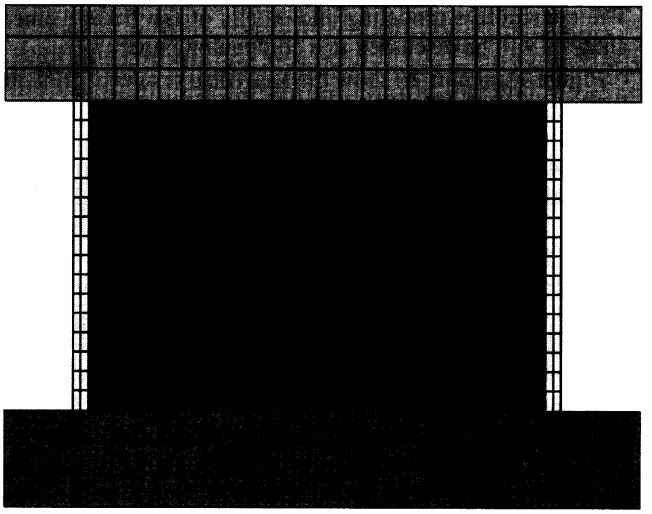

Fig. 12—Finite element mesh for DP test specimens.

Hysteresis trends

The load-displacement results for DP1 and DP2 demonstrated similarities in behavior. Low height-to-width shear walls generally produce hysteresis curves that are highly pinched and demonstrate significantly less energy dissipation than would similar walls with a larger height-to-width ratio. More energy was dissipated through the structure in the post-peak range as the concrete began to soften and the reinforcement yielded locally at cracks. In the pre-peak regime, the concrete within the web wall significantly controlled the response. The observed responses for both DP1 and DP2 were consistent with these general trends.

The load-deformation response for the individual cycles for both specimens demonstrated similar loading and unloading characteristics. The unloading curves of the second excursion at each displacement level generally followed the same unloading path as the first. The shape of the unloading response seemed to be dependent on the strain at the onset of unloading and the residual strain. The residual strains were similar in the two specimens and seemed to be a function of the maximum unloading strain in the history of loading. The reloading lines of the second cycle of displacement followed a similar loading path as the first, but at a lower loading stiffness, resulting in lower peak strengths. The load-deformation curves indicated that the first cycle of a new displacement level followed a very similar loading path to that of the second cycle of the previous displacement. This suggested that further cycles at a specific displacement level would produce negligible damage in comparison with that experienced by the first unloading-reloading cycle, which has also been suggested by other researchers.[13] The response demonstrated this trend until the peak load. During the post-peak response of DP1, the amount of damage experienced during subsequent cycles was significant and similar to that sustained during the second repetition. Specimen DP2 was not able to confirm the latter trend, as it failed in the first excursion of the first cycle within the post-peak range.

Comparisons with NUPEC specimen

Specimen DP1 and the NUPEC specimen U-1 had similar wall geometries and were tested under a similar axial load. The reinforcement in DP1 had approximately double the reinforcement spacing of that of U-1 to maintain a comparable ρf_{sy} ratio. Even though DP1 was tested under static cyclic

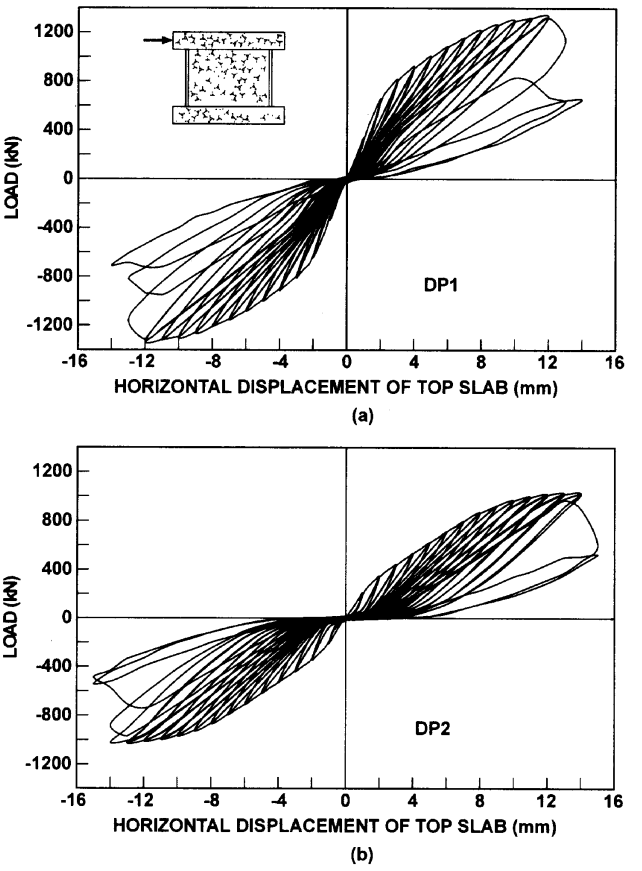

Fig. 13—Predicted load-deformation response: (a) Specimen DP1; and (b) Specimen DP2.

displacements and the NUPEC specimen was tested dynamically, comparisons are possible by investigating the envelope responses of each specimen. (The envelope responses contain the maximum loads at each displacement level.)

The maximum load recorded by NUPEC was 1636 kN at a displacement 10.96 mm; for DP1, the maximum load was 1298 kN at a displacement of 11.14 mm. Specimen U-1 did, however, have a compressive cylinder strength 32% higher than that of DP1. The ratio of U-1 to DP1 peak loads was 1.26. The discrepancy in strength between the two walls was partly related to the difference in the concrete strengths, but was also a function of the ground motion imposed on U-1. The walls did, however, experience a similar amount of ductility. Figure 6(a) and (b) include the envelope response of U-1.

The envelope of U-1 was strongly influenced by the ground motion to which it was subjected. Under seismic conditions, structures do not experience the same straining that they would under a similar static loading, thus producing a stiffer load-displacement response. The envelope responses of U-1 and DP1 indicated that the behaviors were somewhat similar for a specific set of loading conditions, and for this case, static testing seemed to be a viable alternative to dynamic testing.

The modes of failure of the two walls differed significantly; however, both failure mechanisms were the result of the damage experienced in the flange walls. U-1 failed by crushing of the concrete at the toes of the web wall, followed by a sliding shear plane near the base of the wall. The web wall also punched through the flange wall near the base slab. Prior to failure, the flexural reinforcement in the flange walls had yielded, and extensive vertical cracking in the flanges

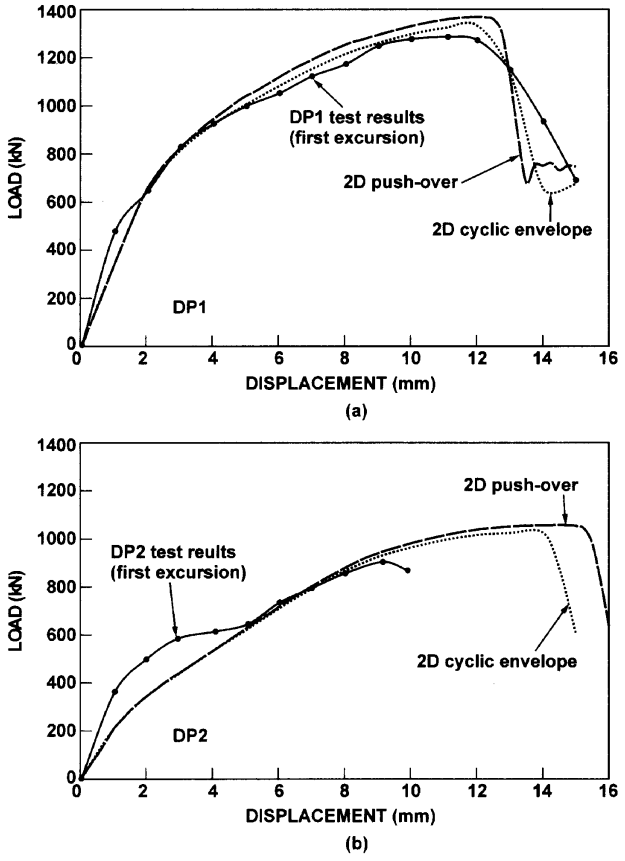

Fig. 14—Comparison of experimental and analytical results: (a) Specimen DP1; and (b) Specimen DP2.

near the web wall was visible. The flanges were significantly damaged and provided little restraint to the formation of a sliding shear failure, whereas the stiff, relatively undamaged flange walls of DP1 restrained the expansion of diagonal cracking in the web wall and caused the formation of vertical slip planes.

ANALYSIS OF WALLS

Vecchio[14] reported an analytical model for reinforced concrete subjected to cyclic loading. The constitutive models for concrete in compression and tension were provisional, and the hysteretic model for the reinforcement was modeled after Seckin.[15] The material models were incorporated into two-dimensional[16] and three-dimensional[17] nonlinear finite element programs based on a smeared, rotating crack model using a secant-stiffness approach. The programs employ the compatibility, equilibrium, and constitutive relationships of the Modified Compression Field Theory.

A two-dimensional static cyclic displacement analysis was performed for DP1 and DP2. The purpose of the analysis was to demonstrate the applicability of a secant-stiffness approach to simulating cyclic loading of reinforced concrete structures. The finite element mesh, shown in Fig. 12, consisted of 540 constant strain rectangular elements. The mesh was divided into four zones: the web wall, flange walls, top slabs, and bottom slabs. The base slab was assumed to be fixed to the laboratory strong floor. Horizontal displacements were imposed on the second nodal joint from the top of the top slab, and the axial load was spread along the bottom two rows of joints in the top slab directly above the walls. The constitutive modeling and details of the finite element analysis will be discussed in a companion paper.

Figure 13(a) and (b) show the analytical results of DP1 and DP2, respectively. For DP1, the results fairly accurately predicted the ultimate strength and the corresponding displacement. Ultimate loads of 1332 kN and –1333 kN were computed by the analysis in the positive and negative directions, respectively. The analysis indicated that the peak loads occurred during Cycle 12 (12 mm of displacement) in the two directions. The analysis results, however, predicted a more dramatic softening effect in the post-peak region, with a significant loss of load capacity occurring during Cycle 13, whereas the experimental response followed a more gradual softening path beyond the peak load. This was a direct result of the post-peak ductility model used for concrete in compression and not a function of the cyclic models. At 13 mm of displacement, the analysis predicted the formation of a sliding shear plane in the web wall near the base slab. Another difference was the higher degree of pinching reported by the analysis. The analysis does, however, confirm that the procedures employed are stable and provide reasonably accurate simulations of the wall's behavior.

The analytical results of DP2 showed somewhat more divergence. The analysis produced ultimate loads of 1027 kN and –1027 kN at displacements of 14 mm and –13 mm, respectively. The predicted failure mechanism involved a sliding shear plane in the web wall near the base slab surfacing at –14 mm of displacement. The analysis was performed assuming that the concrete strength was uniform over the entire height of the wall; however, the actual failure mode of DP2 suggests that the concrete was weaker near the top slab initiating a premature failure in this region. A comparison of the loads at 9 mm of displacement (the last cycle before failure) provided a clearer perspective of the analytical results. The loads recorded by the analysis at 9 mm of displacement were 925 kN and –924 kN. The analysis did, however, predict the energy dissipation and the offsets at unloading when comparing the cycles up to 9 mm of displacement reasonably well.

Results from a monotonic two-dimensional analysis on Specimens DP1 and DP2 are plotted in Fig. 14, along with the envelope response of the two-dimensional cyclic analysis and the experimental (first excursion envelope) response of each specimen. The results indicated that cyclic analysis provided a better estimation of the behavior of the shear walls. Lower peak loads were recorded at each displacement level as a result of the damage incurred by the concrete due to load cycling. The two-dimensional static monotonic response did, however, provide reasonable results and can be used to approximate ultimate loads. A peak load of 1369 kN at a displacement of 12 mm was reported for DP1. For DP2, the results at 9 mm of displacements indicated a lateral resistance of 941 kN.

Even though DP1 and DP2 represent complex wall configurations, the two-dimensional analyses yielded reasonable results. Three-dimensional issues, however, must be addressed, and for DP1 and DP2 this includes the effectiveness of the flange width in contributing to the lateral load resistance of the wall. Concentrating the full width of the flanges into a single element in the two-dimensional model has several significant implications. The very stiff flange elements are assumed to be fully connected to the web elements. Thus, the degree of lateral and vertical confinement they provide to the web can be overestimated. Further, the shear lag effect that occurs in the out-of-plane direction in the three-dimensional

model, in reality, is not considered. Finally, the ability of the flange elements to carry a lateral shear can be overstated when full fixity to the web is assumed. Relative to a three-dimensional analysis, these factors can contribute to overestimating the strength and stiffness of three-dimensional walls and have been confirmed by Vecchio.[18] For DP1 and DP2, however, it appears that the entire width of the flange walls were effective in providing lateral resistance.

CONCLUSIONS

From the experimental program, the following conclusions can be drawn:

1. The experimental results of the shear walls provide detailed information about the behavior of squat shear walls and the influence of applying axial loads;
2. A minimal axial load, 5.4 % of f_c' in the case of DP1, caused a significant increase in the ultimate capacity of the shear wall and influenced the mode of failure;
3. The stiffness of the flange walls was largely responsible for the modes of failure. Stiff flange walls caused vertical slip planes to form in DP1. Possibly, weaker concrete in the upper part of the walls of DP2 caused a zone of weakness near the top slab; the result was a sliding shear failure of the web wall near the top slab;
4. Static cyclic testing is a viable alternative to dynamic testing for the set of loading conditions to which test Specimens DP1 and U-1 were exposed;
5. Squat shear walls produce highly pinched hysteresis curves with little energy dissipation and are more heavily influenced by shear related mechanisms;
6. In the pre-peak cycles (cycles before reaching the maximum lateral load), cycling beyond two excursions to a specific displacement level produces negligible damage in the load-deformation response. In the post-peak region (response after reaching the maximum lateral load), however, the amount of damage in subsequent excursions was similar to that experienced by the first two excursions.

The analysis of reinforced concrete shear walls, using in-house nonlinear finite element analysis programs at the University of Toronto, suggests the following further conclusions:

1. A secant-stiffness based algorithm can be modified to accurately simulate the behavior of reinforced concrete under cyclic loading; and
2. A pushover analysis can generate peak loads and displacements at peak loads within a reasonable range of error; however, a cyclic analysis does provide a better estimation of the expected loads and displacements.

Although the analyses presented demonstrate satisfactory results, improvements to the hysteretic response and ductility models are required. They should include more realistic unloading-reloading curves in compression and tension, damage to the concrete upon reloading, and attention should also be given to modeling partial unloading/partial reloading curves. The data collected from the shear wall tests will be used to corroborate the improved cyclic models for concrete.

NOTATION

f_c' = cylinder compressive strength of concrete
f_{su} = ultimate stress of reinforcement
f_{sy} = yield stress of reinforcement
ε_c' = strain at peak cylinder compressive strength of concrete
ε_{sy} = yield strain of reinforcement
ρ = reinforcement ratio

REFERENCES

1. Nuclear Power Engineering Corporation of Japan, "Comparison Report, Seismic Shear Wall ISP, NUPEC's Seismic Ultimate Dynamic Response Test," *Report* No. NU-SSWISP-D014, Organization for Economic Co-Operation and Development, Paris, 1996, 407 pp.
2. Palermo, D., "Testing of a Three-Dimensional Shear Wall under Cyclic Loading," MASc thesis, Department of Civil Engineering, University of Toronto, Toronto, Ontario, Canada, 1998, 240 pp.
3. Bucci, F., "Finite Element Analysis of Repaired Concrete Structures," MASc thesis, Department of Civil Engineering, University of Toronto, Toronto, Ontario, Canada, 1998, 158 pp.
4. Palermo, D., "Behaviour and Analysis of Reinforced Concrete Walls Subjected to Reversed Cyclic Loading," PhD thesis, Department of Civil Engineering, University of Toronto, Toronto, Ontario, Canada, 2001, 331 pp.
5. Haro de la Peña, O. A., "Modelling and Analysis of Retrofitted Reinforced Concrete Structures," MASc thesis, Department of Civil Engineering, University of Toronto, Toronto, Ontario, Canada, 242 pp.
6. Vecchio, F. J.; Haro de la Peña, O. A.; Bucci, F.; and Palermo, D, "Behavior of Repaired Cyclically Loaded Shear Walls," 17 pp. (submitted for publication)
7. Karsan, D., and Jirsa, J. O., "Behavior of Concrete Under Compressive Loading," *Journal of the Structural Division*, ASCE, V. 95, No. ST12, Dec. 1969, pp. 2543-2563.
8. Lefas, I. D.; Kotsovos, M. D.; and Ambraseys, N. N., "Behavior of Reinforced Concrete Structural Walls: Strength, Deformation Characteristics, and Failure Mechanism," *ACI Structural Journal*, V. 87, No. 1, Jan.-Feb. 1990, pp. 23-31.
9. Sittipunt, S., and Wood, S. L., "Influence of Web Reinforcement on the Cyclic Response of Structural Walls," *ACI Structural Journal*, V. 92, No. 6, Nov.-Dec. 1995, pp. 745-756.
10. Pilakoutas, K., and Elnashai, A., "Cyclic Behavior of Reinforced Concrete Cantilever Walls, Part 1: Experimental Results," *ACI Structural Journal*, V. 92, No. 3, May-June 1995, pp. 271-281.
11. Paulay, T.; Priestley, M. J. N.; and Synge, A. J., "Ductility of Earthquake Resisting Shear Walls," ACI JOURNAL, *Proceedings* V. 79, No. 4, July-Aug. 1982, pp. 257-269.
12. Oesterle, R. G.; Aristizabal-Ochoa, J. D.; Shiu, K. N.; and Corley, W. G., "Web Crushing of Reinforced Concrete Structural Walls," ACI JOURNAL, *Proceedings* V. 81, No. 3, May-June 1984, pp. 231-241.
13. Elnashai, A. S., Pilakoutas, K., and Ambraseys, N. N., "Experimental Behavior of Reinforced Concrete Walls Under Earthquake Loading," *Earthquake Engineering and Structural Dynamics*, V. 19, 1990, pp. 389-407.
14. Vecchio, F. J., "Towards Cyclic Load Modeling of Reinforced Concrete," *ACI Structural Journal*, V. 96, No. 2, Mar.-Apr. 1999, pp. 193-202.
15. Seckin, M., "Hysteretic Behaviour of Cast-in-Place Exterior Beam-Column-Slab Subassemblies," PhD thesis, Department of Civil Engineering, University of Toronto, Toronto, Ontario, Canada, 1981, 266 pp.
16. Vecchio, F. J., "Nonlinear Finite Element Analysis of Reinforced Concrete Membranes," *ACI Structural Journal*, V. 86, No. 1, Jan.-Feb. 1989, pp. 26-35.
17. Vecchio, F. J., and Selby, R. G., "Towards Compression Field Analysis of Reinforced Concrete Solids," *Journal of Structural Engineering*, ASCE, V. 117, No. 6, 1991, pp. 1740-1758.
18. Vecchio, F. J., "Lessons From the Analysis of a Three-Dimensional Concrete Shear Wall," *Structural Engineering and Mechanics*, V. 6, No. 4, 1998, pp. 439-455.